Received: 18 May 2020 | Revised: 24 September 2020 | Accepted: 22 October 2020

DOI: 10.1002/qua.26527

FULL PAPER

International Journal of QUANTUM CHEMISTRY WILEY

Fatigue and fatigue resistance in S_1 excited state diarylethenes in electric fields

Xing Nie | Yong Yang | Tianlv Xu | Steven R. Kirk | Samantha Jenkins

Key Laboratory of Chemical Biology and Traditional Chinese Medicine Research and Key Laboratory of Resource, National and Local Joint Engineering Laboratory for New Petro-Chemical Materials and Fine Utilization of Resources, College of Chemistry and Chemical Engineering, Hunan Normal University, Changsha, China

Correspondence
Steven R. Kirk and Samantha Jenkins, Key Laboratory of Chemical Biology and Traditional Chinese Medicine Research and Key Laboratory of Resource, National and Local Joint Engineering Laboratory for New Petro-Chemical Materials and Fine Utilization of Resources, College of Chemistry and Chemical Engineering, College of Chemistry and Chemical Engineering, Hunan Normal University, Changsha, Hunan 410081, China.
Email: steven.kirk@cantab.net (S. R. K.) and samanthajsuman@gmail.com (S. J.)

Funding information
National Natural Science Foundation of China, Grant/Award Number: 21673071

Abstract

The effect of a directional electric-field on the bonding of the undoped and sulfur doped diarylethene (DTE) switch molecule is investigated using next generation QTAIM (NG-QTAIM). We introduce chemical bonding concepts in the form of the least and most preferred directions of charge density accumulation relative to a bond-path, namely the precessions K and K' that are demonstrated to be much more responsive to the electric-field than the Laplacian $\nabla^2\rho(\mathbf{r}_b)$. A concept of bond fatigue is presented in terms of the tendency for a bond-path to rupture that provides directional versions of familiar bonding QTAIM concepts. Examples of fatigue resistance and fatigue are included where the applied electric-field reduces and increases the tendency toward bond-path rupture respectively. A brief discussion is undertaken of applications of the precessions K and K' including switches, ring opening reactions and molecular rotary motors in the presence of fields that cause a redistribution of $\rho(\mathbf{r})$.

KEYWORDS
diarylethenes, electric-field, excited state, fatigue, next generation QTAIM

ResearchPlatform

1 | INTRODUCTION

The conversion of diarylethene switches (DTE) between a ring-open isomer and the ring-closed isomer by irradiation with UV and visible light is known to possess outstanding properties for technological relevance. In practice DTEs are required to possess highly efficient photoisomerization reactivity and extremely low fatigue over a large number of switching cycles [1,2]. The reality however, is that the stability and longevity of such devices is limited by the robustness of the switches [3] that tend to fatigue after only a few switching cycles [4,5]. Systematic guidelines to relate the chemical structure of DTEs to fatigue resistance have yet to be discovered [6].

In recent years improvements of switching behaviors of DTE structures are usually acquired by a "trial and error" basis of chemical substitutions aimed at tuning the chemical properties of the core of the DTE. Martial Boggio-Pasqua et al proposed that the presence of a conical intersection is central to the photochromic properties of DTEs [1]. Conventionally, the analysis of the DTEs uses the Woodward-Hoffmann rules that are constructed using the conservation of orbital symmetry, that are traditionally used for kinetic and mechanism based investigations of ring-opening reactions [7–9].

Earlier, some of the current authors considered the first excited state (S_1) reactivity of DTEs with developments of (QTAIM) [10] that we refer to as next generation QTAIM (NG-QTAIM) [11] In the previous investigation of DTE, doped and sulfur doped, we mapped out the photochromism and fatigue mechanisms for the passage along internal reaction coordinate pathways in terms of the associated bonds (bond critical points) in a stress tensor space to gain insights into the characteristic behaviors. In particular, we found unfavorable fatigue switch characteristics such as discontinuous and nonreversible behaviors for the undoped DTE fatigue bond but not for the sulfur doped DTE switch fatigue bond. We also demonstrated the insufficiency of the Woodward-Hoffmann rules [8] that use orbital properties for their construction with use of the Schrödinger

 © 2020 Wiley Periodicals LLC

equation. The orbital model has the disadvantage of lacking consistent agreement with experimental data [12]. The understanding of *fatigue* is conventionally understood in terms of the repeatability of switching cycles, with higher fatigue levels being quantified by a lower percentage return to the start (e.g., ring closed position for DTEs) of the switching cycle. The reasons for the differences in switch performance should, we believe, be understood in terms of the intrinsic directional bond properties before the commencement of the switching cycle. In this investigation, therefore we will introduce and define the concept of the precession *K* of the {***p***,***p***′} path-packet, constructed using the least preferred direction of charge density $\rho(\mathbf{r})$ accumulation, associated with a given bond. The DTE fatigue bond determines the tendency toward ring-opening and has an associated ring critical point (*RCP*) located in a geometric ring of atoms. If the {***p***,***p***′} path-packet is directed toward the ring (*RCP*) centre, this indicates a reluctance for the motion of the fatigue bond critical point (*BCP*) toward to *RCP* that would result in the annihilation of both critical points, leading to ring-opening. Earlier, we used the shape of the {***q***,***q***′} and {***p***,***p***′} path-packets to quantify the chemical character, for instance for the double and single bond character of benzene indicated by large and small extents enveloping the *BCP* respectively [13]. The {***q***,***q***′} and {***p***,***p***′} path-packets of the ring-opening reactions of oxirane were twisted and planar for the ground state (S_0) and excited states respectively (S_1) [14]. Mixed chemical character was found using the {***q***,***q***′} and {***p***,***p***′} path-packets for the S_1/S_0 conical intersections of the penta-2,4-dieniminium cation [15]. The presence of twisted {***q***,***q***′} path-packets of benzvalene, produced by following a photochemical excited state reaction path from benzene, indicated a strong C—C bond with characteristics of an unstable weak bond, explaining the known explosive nature of benzvalene [16].

Therefore, in this investigation the main goal is to provide guidelines to relate the chemical structure of DTEs to fatigue and fatigue resistance.

2 | THEORY AND METHODS

2.1 | The QTAIM BCP descriptors; ellipticity ε, the total local energy density $H(\mathbf{r}_b)$

We use QTAIM [10] that utilizes higher derivatives of the total charge density distribution $\rho(\mathbf{r}_b)$ at the bond critical point (*BCP*) where the subscript "**b**" refers to the *BCP*, in effect acting as a "magnifying lens" on the $\rho(\mathbf{r}_b)$ derived properties of the wave-function. QTAIM allows us to identify critical points in the total electronic charge density distribution $\rho(\mathbf{r})$ by analyzing the gradient vector field $\nabla\rho(\mathbf{r})$. These critical points can be divided into four types of topologically stable critical points according to the set of ordered eigenvalues $\lambda_1 < \lambda_2 < \lambda_3$, with corresponding eigenvectors $\underline{\mathbf{e}}_1$, $\underline{\mathbf{e}}_2$, $\underline{\mathbf{e}}_3$ of the Hessian matrix. In the limit that the forces on the nuclei become vanishingly small, an atomic interaction line (AIL) [17] becomes a bond-path, although not necessarily a chemical bond [18]. The complete set of critical points together with the bond-paths of a molecule or cluster is referred to as the molecular graph, with the constituent atoms being referred to as nuclear critical points (*NCPs*). The ellipticity ε provides the relative accumulation of $\rho(\mathbf{r}_b)$ in the two directions perpendicular to the bond-path at a *BCP*, defined as $\varepsilon = |\lambda_1|/|\lambda_2| - 1$ where λ_1 and λ_2 are negative eigenvalues of the corresponding $\underline{\mathbf{e}}_1$ and $\underline{\mathbf{e}}_2$ respectively. The eigenvectors $\underline{\mathbf{e}}_1$ and $\underline{\mathbf{e}}_2$ correspond to the least and most preferred directions of charge density accumulation $\rho(\mathbf{r}_b)$, and the $\underline{\mathbf{e}}_3$ eigenvector is always directed along the bond path. It has been shown [19,20] that the degree of covalent character can be determined from the total local energy density $H(\mathbf{r}_b)$, defined as:

$$H(\mathbf{r}_b) = G(\mathbf{r}_b) + V(\mathbf{r}_b) \tag{1}$$

In Equation **(1)**, $G(\mathbf{r}_b)$ and $V(\mathbf{r}_b)$ are the local kinetic and potential energy densities at a *BCP*, respectively. A value of $H(\mathbf{r}_b) < 0$ for a closed-shell interaction, $\nabla^2\rho(\mathbf{r}_b) > 0$, indicates a *BCP* with a degree of covalent character, and conversely $H(\mathbf{r}_b) > 0$ reveals a lack of covalent character for the closed-shell *BCP*.

The term fatigue bond applies to shared-shell *BCP*s or closed-shell *BCP*s that are in the process of undergoing a ring-opening reaction, where the Laplacian $\nabla^2\rho(\mathbf{r}) > 0$ or Laplacian $\nabla^2\rho(\mathbf{r}) < 0$ (but low) and the total local energy $H(\mathbf{r}_b) \approx 0$. The possible restorative effect on the switching cycle will be investigated by the application of a directional applied **E**-field. The directional properties of NG-QTAIM specify the most ($\underline{\mathbf{e}}_2$) and least ($\underline{\mathbf{e}}_1$) preferred directions of motion of $\rho(\mathbf{r})$ and therefore naturally provide an understanding of "fatigue." In other words, a bond with a larger degree of fatigue will possess a larger associated extent of accumulation of $\rho(\mathbf{r})$ along the most preferred direction ($\underline{\mathbf{e}}_2$) than a bond with a lower degree of fatigue.

2.2 | The QTAIM bond-path properties; the bond-path framework set B, the {*p*,*p*′} path-packet precession *K*

The NG-QTAIM interpretation of the chemical bond as the *bond-path framework set*, denoted by *B*, where *B* = {***p***,***q***,***r***}, with the consequence that for a given electronic state a bond is comprised of three "linkages"; ***p***, ***q*** and ***r*** associated with the $\underline{\mathbf{e}}_1$, $\underline{\mathbf{e}}_2$ and $\underline{\mathbf{e}}_3$ eigenvectors, respectively. Here the ***p*** and ***q*** are 3-D paths constructed from the values of the least ($\underline{\mathbf{e}}_1$) and most ($\underline{\mathbf{e}}_2$) preferred directions of electronic charge density

accumulation $\rho(\mathbf{r})$ along the bond-path, referred to as ($\boldsymbol{r}$). The directions of the $\boldsymbol{p}$-, $\boldsymbol{q}$- and $\boldsymbol{r}$-paths always remain orthogonal to each other because they are constructed from the $\underline{\mathbf{e}}_1$, $\underline{\mathbf{e}}_2$ and $\underline{\mathbf{e}}_3$ eigenvectors respectively. The ellipticity ε is used a scaling factor in the construction of the $\boldsymbol{p}$- and $\boldsymbol{q}$-paths:

$$\boldsymbol{p}_i = \boldsymbol{r}_i + \varepsilon_i \underline{\mathbf{e}}_{1,i}$$

$$\boldsymbol{q}_i = \boldsymbol{r}_i + \varepsilon_i \underline{\mathbf{e}}_{2,i} \tag{2}$$

In the limit of vanishing ellipticity $\varepsilon = 0$, *for all* steps i along the bond-path then H = BPL, the lengths of the $\boldsymbol{p}$- and $\boldsymbol{q}$-paths are defined as the *eigenvector-following paths* H^* or H:

$$H* = \sum_{n-1}^{i=1} |\boldsymbol{p}_{i+1} - \boldsymbol{p}_i|$$

$$H = \sum_{n-1}^{i=1} |\boldsymbol{q}_{i+1} - \boldsymbol{q}_i| \tag{3}$$

The extent that the pair of $\boldsymbol{q}$- and $\boldsymbol{q}'$-paths form along the *BCP* are referred to as a $\{\boldsymbol{q},\boldsymbol{q}'\}$ path-packet, the imminent *rupture* of a *BCP* is caused by the coalescence with the associated *RCP* and is predicted by extremely long $\{\boldsymbol{q},\boldsymbol{q}'\}$ or $\{\boldsymbol{p},\boldsymbol{p}'\}$. The greater readiness of a *BCP* to move is indicated by larger $\{\boldsymbol{q},\boldsymbol{q}'\}$ path-packets in the vicinity of a *BCP*. An in depth discussion with derivations of B = $\{\boldsymbol{p},\boldsymbol{q},\boldsymbol{r}\}$ is provided in the Supporting Information S1. The excess lengths (H, H') and (H^*, $H^{*\prime}$) of the $\{\boldsymbol{p},\boldsymbol{p}'\}$ and $\{\boldsymbol{q},\boldsymbol{q}'\}$ path-packets respectively compared with the bond-path lengths (BPL) and inter-nuclear separations (GBL) provide the NG-QTAIM interpretation of the response of the applied **E**-field.

2.3 | The QTAIM bond-path properties; the $\{p,p'\}$ and $\{q,q'\}$ path-packet precession K and K'

In this investigation we seek to quantify the response to a directional (±) applied **E**-field on the undoped and sulfur doped DTE molecule in terms of the extent the $\{\boldsymbol{p},\boldsymbol{p}'\}$ and $\{\boldsymbol{q},\boldsymbol{q}'\}$ path-packets "wrap" or precess around the associated bond-path. This will be undertaken in terms of the tendency toward the discontinuous and nonreversible behavior of bond rupture, *bond-path fatigue*, or the resistance to this rupturing process, *bond-path fatigue resistance*. Bonds will rupture if the *BCP* and *RCP* coalesce, as this process unfolds most readily when the $\underline{\mathbf{e}}_2$ eigenvector that indicates the most facile direction, for example, of the fatigue bond *BCP* will align along the *BCP*→ *RCP* path. The maximum tendency to *avoid BCP* and *RCP* coalescence occurs when the $\underline{\mathbf{e}}_1$ eigenvector, that indicates the least facile, most resistant direction, is parallel/anti-parallel to the *BCP*→ *RCP* path, denoted by the gray line in Scheme 1. We will now define the extent to which the $\{\boldsymbol{p},\boldsymbol{p}'\}$ path-packet, constructed from the $\underline{\mathbf{e}}_1$ eigenvector, *precesses* about the fatigue closed-shell C5—C11 *BCP* bond-path and the fatigue shared-shell C5—S26 *BCP* bond-path, see the left and right panels of Scheme 1 respectively.

For the $\{\boldsymbol{p},\boldsymbol{p}'\}$ path-packet, defined by the $\underline{\mathbf{e}}_1$ eigenvector, we wish to follow the extent to which the $\{\boldsymbol{p},\boldsymbol{p}'\}$ path-packet precesses about the bond-path by defining the *precession* K for the bond-path fatigue:

$$K = 1 - \cos^2\alpha, \text{where } \cos\alpha = \underline{\mathbf{e}}_1 \cdot \underline{\mathbf{u}} \text{ and } 0 \le K \le 1 \tag{4}$$

Considering the extremes, K = 0 we have a minimum degree of closed-shell *BCP* character and for K = 1 we have the maximum degree of closed-shell *BCP* character. Values of K = 0 and K = 1 also indicate the lowest and highest tendencies toward bond-path fatigue respectively.

The precession K is determined relative to the *BCP*, in either direction along the bond-path toward the nuclei at either ends of the bond-path from an arbitrarily small spacing of $\underline{\mathbf{e}}_1$ eigenvectors. If we chose the precession of the $\{\boldsymbol{p},\boldsymbol{p}'\}$ path-packet about the bond-path when the $\pm\underline{\mathbf{e}}_1$

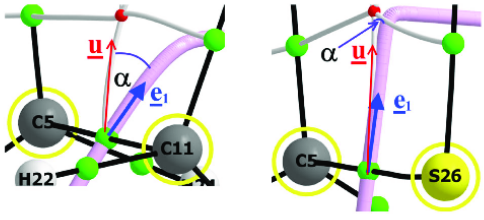

SCHEME 1 The $\{\boldsymbol{p},\boldsymbol{p}'\}$ path-packet precession K construction, $\underline{\mathbf{u}}$ is a unit vector (red arrow) along the *BCP*→ *RCP* path denoted by the gray line, the $\underline{\mathbf{e}}_1$ eigenvector (blue arrow). Shown highlighted by the yellow circles is the closed-shell C5—C11 *BCP* fatigue bond (left panel) and the shared-shell C5—S26 *BCP* fatigue bond (right panel). The undecorated red and green spheres indicate the locations of the bond critical points (*BCP*s) and ring critical points (*RCP*s) respectively. The pale magenta line indicates the interatomic surface path (IAS) that originates at the *BCP*

Rights Option

eigenvector is parallel to $\underline{\mathbf{u}}$, that defines the *BCP*→*RCP* path, the *BCP* will have minimum closed-shell character, see Scheme 1. By following the variation of the precession *K* we can quantify the degree of closed-shell *BCP* character along an entire bond-path.

For the precession of the {***q***,***q***′} path-packet, defined by the $\underline{\mathbf{e}}_2$ eigenvector, about the bond-path, $\beta = (\pi/2 - \alpha)$ and α is defined by Equation (4) see Scheme 1, we can write an expression *K*′ for the bond-path fatigue resistance:

$$K' = 1 - \cos^2\beta, \text{where } \cos\beta = \underline{\mathbf{e}}_2 \cdot \underline{\mathbf{u}},\ \beta = (\pi/2 - \alpha) \text{ and } 0 \le K' \le 1 \tag{5}$$

Note, for the general case the $\underline{\mathbf{e}}_3$ eigenvector defined along the bond-path is not perpendicular to the reference direction $\underline{\mathbf{u}}$, see Scheme 2. For *K*′ = 0 we have a minimum degree of shared-shell character and for *K* = 1 we have the maximum degree of shared-shell character and values of *K*′ = 0 and *K*′ = 1 also indicate bond-paths with the lowest and highest tendencies toward fatigue resistance respectively.

Now it is possible to express the {***p***,***p***′} and {***q***,***q***′} path-packets in both in terms of the lengths (*H**,*H**′),(*H*,*H*′) respectively, along with the precession *K* and *K*′, compactly expressed as ((*H**,*H**′), *K*) and ((*H*,*H*′), *K*′) respectively.

3 | COMPUTATIONAL DETAILS

The molecular structure was optimized with Gaussian 09 [21] using CAS (10,10)/6-31G* and CAS (14,12)/6-31G* for the undoped and sulfur doped DTE switch respectively. The active spaces and corresponding orbitals were chosen in keeping with our previous work [11] and in consultation with other authors of previous work in this field [22]. The settings were retained and the converged geometry (nuclear positions) kept fixed in all subsequent calculations. Single-point SCF calculations were then performed with the aforementioned theory settings and basis set, using additional stricter convergence criteria; $<10^{-10}$ RMS difference in the density matrix and $<10^{-8}$ maximum difference in the density matrix, where a range of external electric field values (−0.02 au, 0, +0.02 au) is applied with values chosen to be accessible experimentally, for example, using scanning tunneling microscope.

Care was taken to ensure consistency of the $+\boldsymbol{E}_{\mathbf{para}}$ corresponding to the C5 → C11 direction and $-\boldsymbol{E}_{\mathbf{para}}$ to C5 ← C11 and similarly for the $+\boldsymbol{E}_{\mathbf{para}}$ ($-\boldsymbol{E}_{\mathbf{para}}$) corresponded to the C5 → S26 (C5 ← S26) directions, aligned along the Cartesian ±*x*-axis, with the *z*-axis defined as being perpendicular to the plane of the —C5—C3—C9—C7—C11— and —C5—C3—C9—C7—S26— rings for the undoped and sulfur doped DTE structures respectively. We used the conventional definition of the field direction [23] used by Gaussian 09, consistent with earlier literature [24]. These calculations yielded the wave-functions needed for NG-QTAIM analysis. Calculations of the molecular graphs and critical point properties were performed using AIMAll [25]. All molecular graphs were additionally confirmed to be free of non-nuclear attractor critical points.

© Right Platform

4 | RESULTS AND DISCUSSIONS

4.1 | The relative BCP shifts, bond-path ellipticity profiles ε and the {*q*,*q*′} and {*p*,*p*′} path-packets

In this section we will examine the scalar and vector responses of fatigue bonds of the undoped DTE and sulfur doped DTE structures subjected to a directed $\boldsymbol{E}_{\mathbf{para}}$-field = ±0.02 a.u. The corresponding values for $\boldsymbol{E}_{\mathbf{perp}}$-field = ± 0.02 au $\boldsymbol{E}_{\mathbf{perp}}$-field = 0 are presented in the Supporting Information S2. The movement of the *BCP*s relative to the absence of an applied **E**-field, along the containing bond-paths for the undoped and sulfur doped DTE molecular graphs are presented in Figure 1A,B respectively.

The direction of the *BCP* movement for the fatigue C5 → C11 *BCP* bond-path for the undoped DTE is aligned along $\boldsymbol{E}_{\mathbf{para}}$-field = ± 0.02 au, seen as the black arrow, see Figure 1A. The converse is observed for the fatigue C5 → S26 *BCP* bond-path for the sulfur doped DTE (yellow arrow), see Figure 1B. For both the undoped and sulfur doped DTE the application of the $\boldsymbol{E}_{\mathbf{para}}$-field = ± 0.02 au causes significant relative motion of the *BCP*s away from the site of the fatigue bonds despite the very low relative distortion of the BPLs, see Tables 1 and 2.

Apart from the fatigue bonds for the undoped and sulfur doped DTE there are no readily discernable trends that explain the effect of the applied $\boldsymbol{E}_{\mathbf{para}}$-field on the relative motion Δ(C—*BCP*) and Δ(*BCP*—C/S) of the *BCP*s along the bond-paths. Therefore, we will now consider the

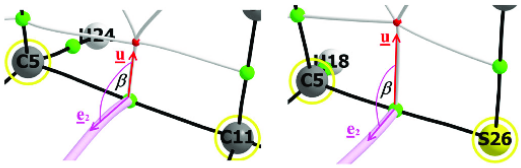

SCHEME 2 The {***q***,***q***′} path-packet precession *K*′ construction, $\underline{\mathbf{u}}$ is a unit vector (red arrow) along the *BCP*→ *RCP* path denoted by the gray line, the $\underline{\mathbf{e}}_2$ eigenvector (magenta arrow), the ± sign of $\underline{\mathbf{e}}_2$ is chosen to form the right handed orthogonal set {$\underline{\mathbf{e}}_2$, $\underline{\mathbf{e}}_2$, $\underline{\mathbf{e}}_3$} and the angle $\beta = (\pi/2 - \alpha)$, see the caption of Scheme 1

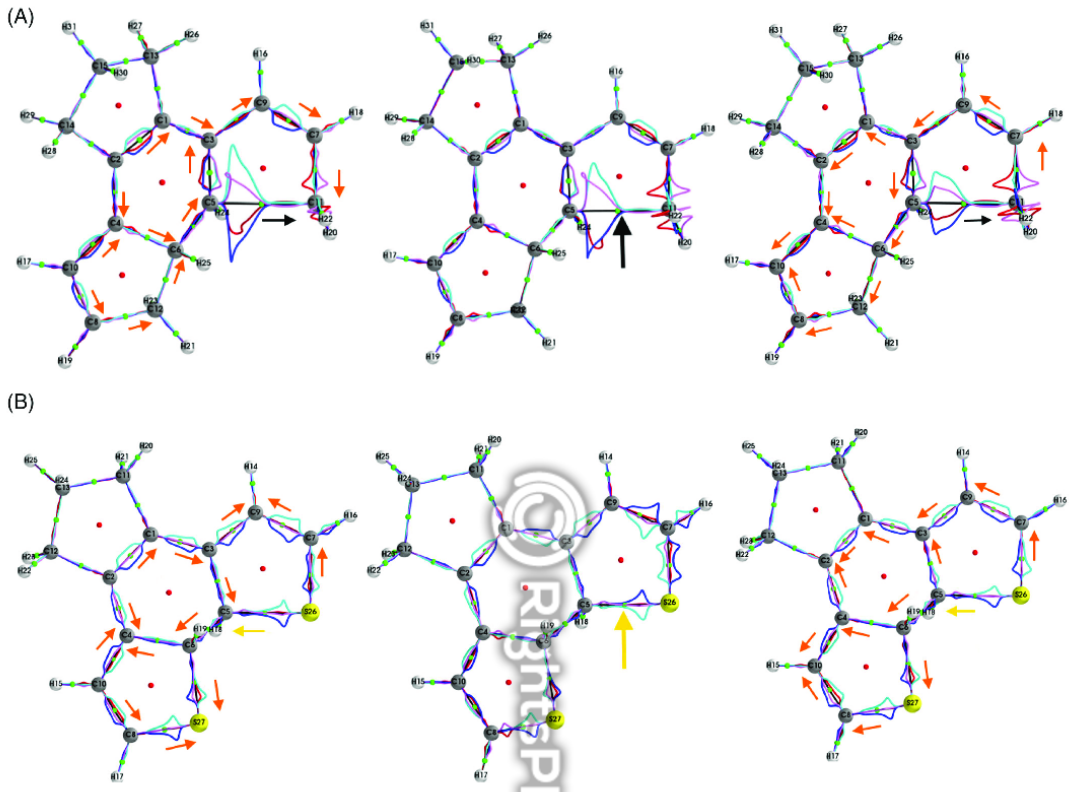

FIGURE 1 The relative movement (arrows not to scale) of the non-fatigue bond critical points (*BCPs*) (orange arrows) {***q***,***q***′} path-packets (magenta, red) and {***p***,***p***′} path-packets (light-blue, dark-blue) of the undoped DTE fatigue C5—C11 *BCP* (black arrow) of the $\boldsymbol{E}_{\text{para}}$-field = −0.02 au (left panel), $\boldsymbol{E}_{\text{para}}$-field = 0 (middle panel) and $\boldsymbol{E}_{\text{para}}$-field = +0.02 au (right panel) are presented in sub-figure (A). The {***q***,***q***′} and {***p***,***p***′} path-packets correspond to the most preferred and least preferred directions of charge density accumulation $\rho(\mathbf{r})$ respectively. The corresponding results for the sulfur doped DTE fatigue C5—S26 *BCP* (yellow arrow), are presented in sub-figure (B) with $\boldsymbol{E}_{\text{para}}$-field = −0.02 au (left panel), $\boldsymbol{E}_{\text{para}}$-field = 0 (middle panel) and $\boldsymbol{E}_{\text{para}}$-field = +0.02 au (right panel)

effect of the ellipticity ε profiles on the bonding that captures the tendency for the charge density $\rho(\mathbf{r})$ to accumulate around the plane of the *BCP*. The application of an electric $\boldsymbol{E}_{\text{para}}$-field = +0.02 a.u parallel to the C5 → C11 *BCP* bond-paths causes a reduction of the C5—C11 *BCP* bond-path ellipticity ε profiles in the DTE switch, see Figure 2A. Reversing the direction of the $\boldsymbol{E}_{\text{para}}$-field = +0.02 a.u parallel, however, does not yield a distinct change in the ellipticity ε profile of the C5 ← C11 *BCP* bond-path. The corresponding $\boldsymbol{E}_{\text{para}}$-field = ± 0.02 au results for the sulfur doped DTE can be seen to reduce the C5 → S26/C5 ← S26 *BCP* bond-path ellipticity ε profiles relative to the absence of the **E**-field, see Figure 2A. Therefore we now consider for the undoped and sulfur doped DTE switch the relative eigenvector following paths lengths ΔH and $\Delta H^{*\prime}$ associated with the ***q***-path and ***p***′-path respectively, see Tables 3 and 4 respectively. For the undoped DTE we observe large negative values for ΔH and $\Delta H^{*\prime}$ corresponding to the fatigue C5—C11 *BCP* bond-path subjected to $\boldsymbol{E}_{\text{para}}$-field = 0.02 au, the remaining *BCPs* display at least an order or magnitude lower response. The response of the ΔH and $\Delta H^{*\prime}$ to $\boldsymbol{E}_{\text{para}}$-field = −0.02 au is lower although the C7—C11 *BCP* indicates a greater response than the fatigue C5—C11 *BCP* bond-path.

The significantly higher response of the ΔH and $\Delta H^{*\prime}$ values subject to $\boldsymbol{E}_{\text{para}}$-field = 0.02 au compared with $\boldsymbol{E}_{\text{para}}$-field = −0.02 au is consistent with the ellipticity ε profile values, see Figure 2A. The results for the sulfur doped show a greater tendency toward including a spreading of the response of the ΔH and $\Delta H^{*\prime}$ values and again the results are consistent with the ellipticity ε profile values, see Figure 2B.

The corresponding changes (reduction/increase) in the associated {***q***,***q***′} and {***p***,***p***′} path-packets are relative to **E**-field = 0 for the undoped and sulfur doped fatigue bond-paths, remembering that the ellipticity ε is the scaling factor used in the construction of the {***q***,***q***′} and {***p***,***p***′} path-packets, see Figure 2A,B respectively. The consideration of the ellipticity profiles ε does not provide the directional information required to determine the tendency toward bond-path fatigue resistance that requires knowledge of the resistance of the *BCP* to move toward the *RCP* causing

	ΔE_{para} = −0.02 au		ΔE_{para} = +0.02 au	
	Δ(C—*BCP*), Δ(*BCP*—C)	Δ(BPL)	Δ(C—*BCP*), Δ(*BCP*—C)	Δ(BPL)
C5—*BCP*, *BCP*—C11	(0.0227, −0.0226)	−0.002	(0.0293, −0.0295)	−0.002
C7—*BCP*, *BCP*—C11	(0.0171, −0.0171)	0.000	(−0.0118, 0.0118)	0.000
C5—*BCP*, *BCP*—C3	(0.0044, −0.0042)	0.000	(−0.0167, 0.0167)	0.000
C9—*BCP*, *BCP*—C7	(0.0238, −0.0238)	0.000	(−0.0298, 0.0300)	0.001
C5—*BCP*, *BCP*—C6	(−0.0256, 0.0257)	0.000	(0.0297, −0.0298)	0.001
C3—*BCP*, *BCP*—C9	(0.0576, −0.0574)	0.001	(−0.0515, 0.0513)	0.000
C6—*BCP*, *BCP*—C12	(−0.0177, 0.0176)	0.000	(0.0191, −0.0189)	0.000
C8—*BCP*, *BCP*—C12	(0.0422, −0.0422)	0.000	(−0.0443, 0.0443)	0.000
C10—*BCP*, *BCP*—C4	(0.0361, −0.0357)	0.001	(−0.0340, 0.0337)	0.000
C10—*BCP*, *BCP*—C8	(0.0134, −0.0128)	0.001	(−0.0088, 0.0085)	0.001
C6—*BCP*, *BCP*—C4	(−0.0400, 0.0399)	0.000	(0.0386, −0.0385)	0.000
C4—*BCP*, *BCP*—C2	(−0.0010, 0.0014)	−0.001	(−0.0104, 0.0103)	−0.000
C2—*BCP*, *BCP*—C1	(0.0205, −0.0206)	0.000	(−0.0172, 0.0174)	0.000
C1—*BCP*, *BCP*—C3	(0.0451, −0.0453)	0.000	(−0.0529, 0.0530)	0.000

TABLE 1 The undoped diarylethene (DTE) switch relative partial bond-path lengths Δ(C—*BCP*) and Δ(*BCP*—C) along with the associated Δ(BPL), in a.u. for the applied E-fields; ΔE_{para} = ± 0.02 au and ΔE_{perp} = ± 0.02 au are presented. The relative partial bond-path lengths Δ(C—*BCP*) and Δ(*BCP*—C) were calculated by subtracting off the corresponding E-field = 0 values, the original bond-path lengths (BPLs) and partial BPLs are provided in the Supporting Information S4

	ΔE_{para} = −0.02 au		ΔE_{para} = +0.02 au	
	Δ(C—*BCP*), Δ(*BCP*—S/C)	Δ(BPL)	Δ(C—*BCP*), Δ(*BCP*—S/C)	Δ(BPL)
C5—*BCP*, *BCP*—S26	(−0.0206, 0.0204)	0.006	(−0.0697, 0.0697)	0.000
C7—*BCP*, *BCP*—S26	(−0.0141, 0.0140)	0.000	(−0.0005, 0.0007)	0.000
C9—*BCP*, *BCP*—C7	(−0.0121, 0.0121)	0.000	(−0.0416, 0.0416)	0.000
C5—*BCP*, *BCP*—C6	(0.0083, −0.0084)	0.001	(0.0598, −0.0590)	0.002
C5—*BCP*, *BCP*—C3	(−0.0175, 0.0175)	0.001	(0.0257, −0.0255)	0.001
C3—*BCP*, *BCP*—C9	(0.0144, −0.0143)	0.000	(−0.0332, 0.0331)	0.000
C6—*BCP*, *BCP*—S27	(0.0238, −0.0238)	0.000	(0.0066, −0.0065)	0.000
C8—*BCP*, *BCP*—S27	(0.0123, −0.0123)	0.000	(−0.0717, 0.0717)	0.001
C10—*BCP*, *BCP*—C8	(0.0364, −0.0361)	0.001	(−0.0270, 0.0270)	0.000
C10—*BCP*, *BCP*—C4	(0.0499, −0.0495)	0.000	(−0.0281, 0.0280)	0.000
C6—*BCP*, *BCP*—C4	(0.0172, −0.0173)	0.000	(0.0477, −0.0477)	−0.001
C4—*BCP*, *BCP*—C2	(−0.0790, 0.0792)	0.000	(0.0287, −0.0289)	−0.001
C2—*BCP*, *BCP*—C1	(0.0092, −0.0095)	0.000	(−0.0392, 0.0394)	0.000
C1—*BCP*, *BCP*—C3	(0.0112, −0.0111)	0.000	(−0.0545, 0.0545)	0.000

TABLE 2 The sulfur doped diarylethene (DTE) switch relative Δ(C—*BCP*) and Δ(*BCP*—S/C) partial bond-path lengths along with the associated Δ(BPL), in a.u. for the applied E-fields; ΔE_{para} = ± 0.02 au and ΔE_{perp} = ± 0.02 au are presented, see the caption of Table 1 for further details, the original bond-path lengths (BPLs) and partial BPLs are provided in the Supporting Information S4

the annihilation of both critical points. In other words, the scalar nature of ellipticity ε does not provide sufficient information to enable the prediction of the tendency toward or away from fatigue resistance a candidate fatigue bond would possess.

In the next section we consider the directional information provided by the precessions K and K' of the $\{p,p'\}$ and $\{q,q'\}$ path-packets respectively for a selection of the DTE bond-paths.

4.2 | Bond-path fatigue K and the bond-path fatigue resistance K' of the undoped and sulfur doped DTE

In this section we track the rotation of the least ($\underline{e}_1$) and most ($\underline{e}_2$) preferred eigenvector about the bond-path that we refer to as the precessions K and K' of the $\{p,p'\}$ and $\{q,q'\}$ path-packets respectively, see Equation **(4)** and Equation **(5)** in the theory background Section 2.3, for the undoped and sulfur doped DTE molecular graphs, see Figures 3–6. The precession K of the $\{p,p'\}$ path-packet defines the bond-path fatigue and correspondingly the precession K' of the $\{q,q'\}$ defines the bond-path fatigue resistance. The precession K provides a bounded definition of the minimum (K = 0) and maximum (K = 1) degree of closed-shell *BCP* character respectively, along an entire bond-path, excluding the nuclear coordinates,

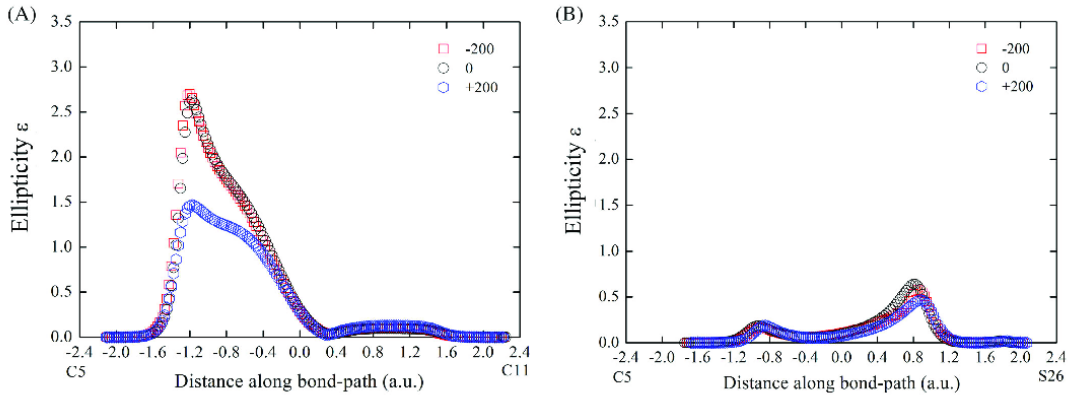

FIGURE 2 The C5—C11 bond critical point (*BCP*) bond-path ellipticity ε profiles in the S_1 state, for the undoped diarylethene (DTE) switch for values of the E_{para}-field = −0.02 au (red), E_{para}-field = 0 (black) and E_{para}-field = +0.02 au (blue) are presented in sub-figure (A), the electric (E_{para})-field is aligned parallel/anti-parallel in the undoped (C5 → C11/C5 ← C11). The corresponding fatigue C5—S26 *BCP* bond-path ellipticity ε profiles in the S_1 state, for the undoped diarylethene (DTE) are presented in sub-figure (B)

RightsPlatform

TABLE 3 The variation of the differences in lengths of the undoped diarylethene (DTE) switch of eigenvector following path lengths ΔH (length of the q-path) and $\Delta H^{*\prime}$ (length of the p'-path), with values of the external E_{para}-field = ±0.02 au. In addition, the total local energy density $\Delta H(r_b)$ are provided, all units are in au, the E-field = 0 values are subtracted

	ΔE_{para} = −0.02 au			ΔE_{para} = +0.02 au		
BCP	ΔH	$\Delta H^{*\prime}$	$\Delta H(r_b)$	ΔH	$\Delta H^{*\prime}$	$\Delta H(r_b)$
C5—C11	0.151	0.117	0.001	−2.216	−2.059	0.000
C7—C11	−0.621	−0.623	−0.002	0.019	0.020	0.003
C5—C3	0.060	0.061	0.001	0.109	0.102	−0.003
C9—C7	−0.001	−0.006	−0.002	0.003	0.006	0.000
C5—C6	0.016	0.015	0.000	0.052	0.050	−0.001
C3—C9	0.012	0.013	−0.003	0.017	0.017	−0.002
C6—C12	−0.001	−0.002	0.000	0.010	0.010	0.000
C8—C12	−0.054	−0.057	−0.002	0.020	0.022	−0.001
C10—C4	0.029	0.034	0.001	−0.012	−0.013	−0.004
C10—C8	0.000	0.003	0.003	−0.007	−0.009	−0.002

TABLE 4 The variation of the differences in lengths of the sulfur doped diarylethene (DTE) switch of eigenvector following path length ΔH (length of the q-path) and $\Delta H^{*\prime}$ (length of the p'-path) with values of the external E-field = −0.02 au and + 0.02 au. In addition, the total local energy density $\Delta H(r_b)$ are provided, all units are in au, the E-field = 0 values are subtracted

	ΔE_{para} = −0.02 au			ΔE_{para} = +0.02 au		
BCP	ΔH	$\Delta H^{*\prime}$	$\Delta H(r_b)$	ΔH	$\Delta H^{*\prime}$	$\Delta H(r_b)$
C5—S26	−0.069	−0.095	0.000	−0.227	−0.237	0.003
C7—S26	−0.436	−0.436	0.000	−0.456	−0.448	0.002
C9—C7	−0.400	−0.394	−0.007	−0.609	−0.597	−0.002
C5—C6	0.000	0.003	0.006	0.051	0.060	−0.003
C5—C3	0.009	0.009	0.001	0.050	0.058	−0.001
C3—C9	−0.012	−0.007	0.001	−0.124	−0.129	0.001
C6—S27	0.051	0.051	−0.002	0.074	0.074	0.000
C8—S27	−0.200	−0.192	−0.001	−0.271	−0.263	0.007
C10—C8	0.064	0.064	0.008	0.195	0.187	−0.004
C10—C4	0.067	0.071	0.002	0.046	0.036	−0.002

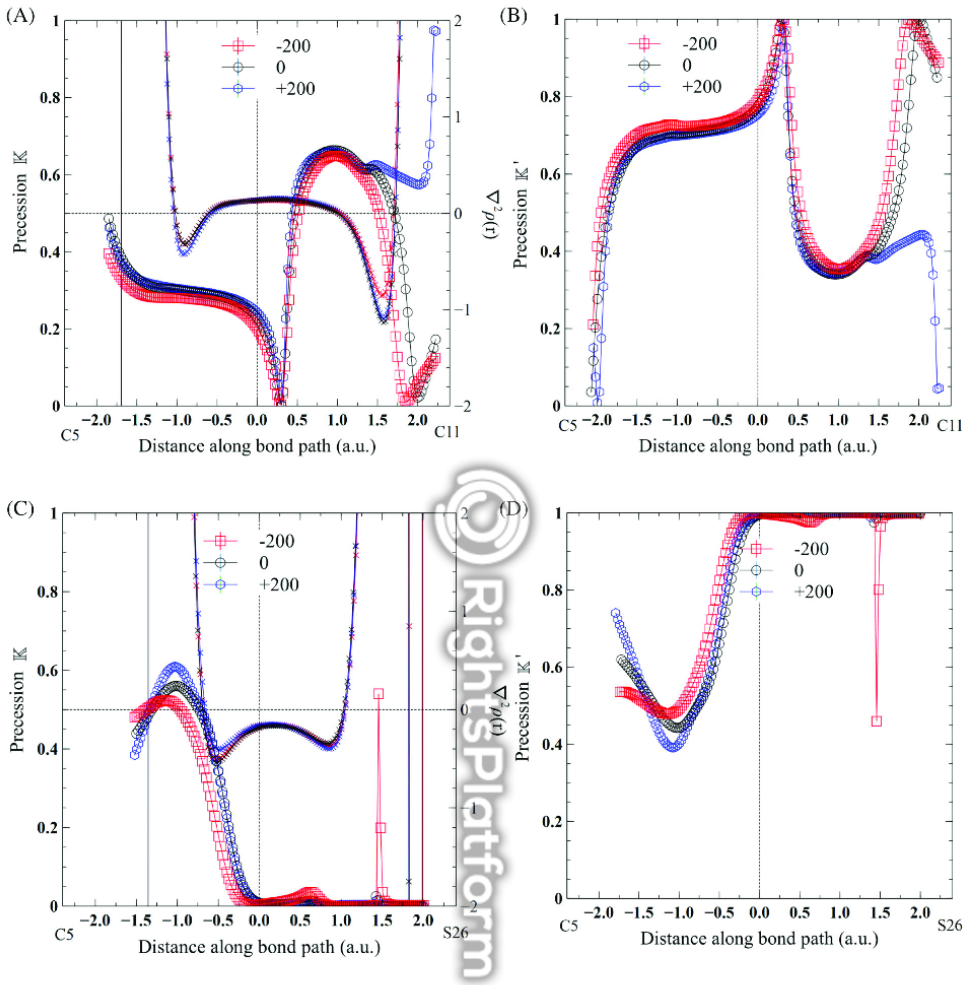

FIGURE 3 The values of the undoped diarylethene (DTE) fatigue C5—C11 bond critical point (*BCP*) bond-path {***p***,***p***′} and {***q***,***q***′} path-packet precession *K* and *K*′ are presented in sub-figure (A) and (B) respectively. The values of the fatigue sulfur doped C5—26 *BCP* bond-path {***p***,***p***′} and {***q***,***q***′} precession *K* and *K*′ are presented in sub-figure (C) and (D) respectively. The electric $\boldsymbol{E}_{\mathbf{para}}$-field = −0.02 au (red), $\boldsymbol{E}_{\mathbf{para}}$-field = 0 (black) and $\boldsymbol{E}_{\mathbf{para}}$-field = +0.02 au (blue) are presented in sub-figure (A), the $\boldsymbol{E}_{\mathbf{para}}$-field is aligned parallel/anti-parallel in the undoped (C5 → C11/C5 ← C11) and sulfur doped (C5 → S26/C5 ← S26), see Figure 1 for the atomic labels, The vertical dashed lines at a distance of 0.0 au indicates the position of the fatigue C5—C11/C5—S26 *BCP* for an **E**-field = 0. The Laplacian values are provided on the right hand y-axis, the horizontal dashed line indicates values of $\nabla^2\rho(\mathbf{r}_b) = 0$. The *K* values corresponding to the positions of the C5 and C11/S26 atoms are not included on the x-axis because the corresponding eigenvectors are not associated with the bond-path

note that the location of the *BCP* is indicated by the vertical dotted line. The precession *K* is presented along with the Laplacian $\nabla^2\rho(\mathbf{r})$, where from conventional QTAIM it is known that at the *BCP* values of $\nabla^2\rho(\mathbf{r}_b) < 0$ and $\nabla^2\rho(\mathbf{r}_b) < 0$ indicate shared-shell *BCP* and closed-shell *BCP* respectively. The precession *K*′ provides a bounded definition of the minimum (*K*′ = 0) and maximum (*K*′ = 1) degree of shared-shell *BCP* character respectively, along an entire bond-path, excluding the nuclear coordinates. The corresponding values for $\boldsymbol{E}_{\mathbf{perp}}$-field = ± 0.02 au for the fatigue bonds are presented in Figure S2D. In addition to the fatigue we chose a selection of bond-paths, C7—C11/C7—S26 *BCP*, C6—C12/C6—S27 *BCP* and C7—C9 *BCP*, on the basis of possessing different orientations relative to the applied $\boldsymbol{E}_{\mathbf{para}}$-field, see Figures 4–6 respectively.

It can be observed that the *K* values corresponding to the fatigue C5—C11/C5—S26 *BCP* bond-paths show a greater variation with the direction (+) or (−) for the $\boldsymbol{E}_{\mathbf{perp}}$-field compared with the $\boldsymbol{E}_{\mathbf{para}}$-field. This is because of the different relative orientations of the ($\underline{\mathbf{e}}_1$) and ($\underline{\mathbf{e}}_2$) with the

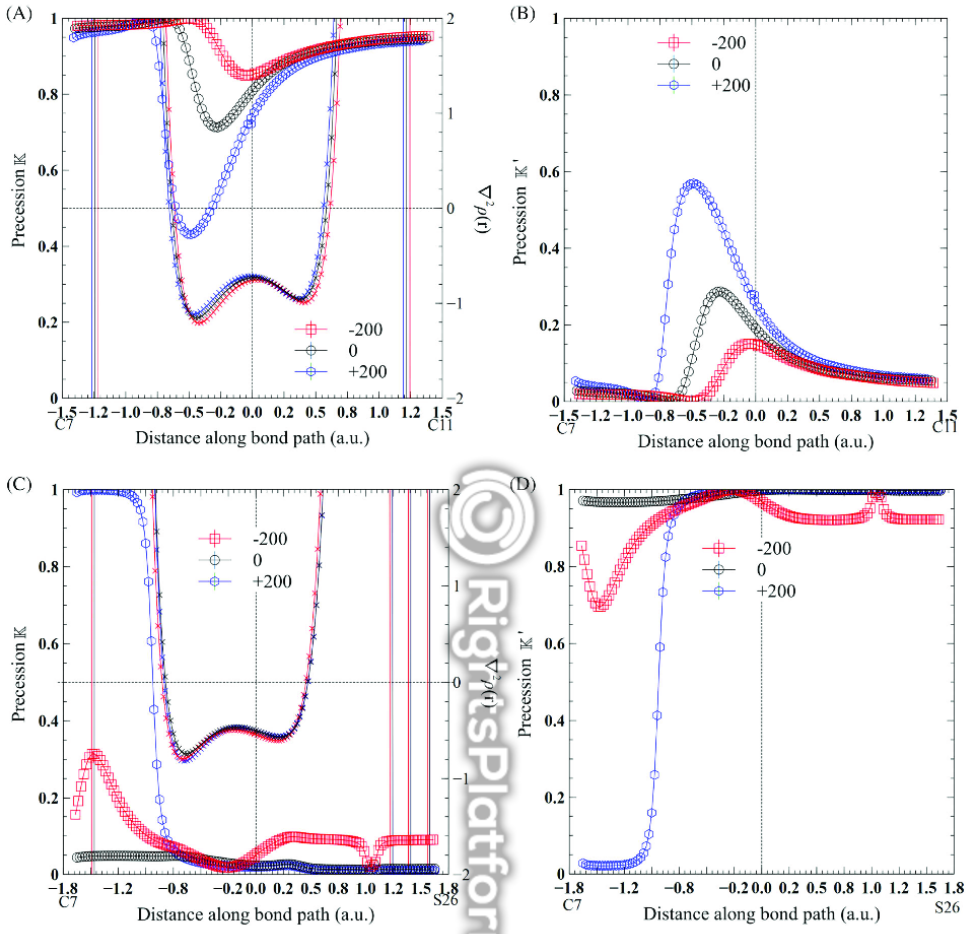

RightsPlatform

FIGURE 4 The values of the C7—C11 bond critical point (*BCP*) bond-path {***p***,***p***′} and {***q***,***q***′} path-packet precession *K* and *K*′ for the undoped diarylethene (DTE) are presented in sub-figure (A) and (B) respectively. The values of the C7—26 *BCP* bond-path {***p***,***p***′} and {***q***,***q***′} precession *K* and *K*′ for the sulfur doped DTE are presented in sub-figure (C) and (D) respectively, see the caption of Figure 3 for further details

$\boldsymbol{E}_{perp}$-field and the $\boldsymbol{E}_{para}$-field. The vertical bands on the left and right hand sides of each of sub-figure A in Figures 3–6 correspond to large values of the Laplacian $\nabla^2\rho(\mathbf{r})$.

We do not repeat, for clarity, the $\nabla^2\rho(\mathbf{r})$ plots for the corresponding *K*′ that are presented in sub-figures B in Figures 3–6. It can be seen that the values of $\nabla^2\rho(\mathbf{r})$ are somewhat invariant to the magnitude or direction of the applied **E**-field. The form of the profile of $\nabla^2\rho(\mathbf{r})$ are very similar for all the bonds, however this is not the case for the precessions *K* and *K*′ of the {***p***,***p***′} and {***q***,***q***′} path-packets.

In the approximate range ± 0.8 au either side of the DTE fatigue closed-shell C5—C11 *BCP*, the chemical character transforms to shared-shell character, indicated by the presence of Laplacian $\nabla^2\rho(\mathbf{r}) < 0$, see the right hand axis of Figure 3A. The DTE fatigue closed-shell C5—C11 *BCP* however, in the absence of an **E**-field contains a degree of shared-shell covalent character indicated by $H(\mathbf{r}_b) = -0.008$ au, that is, $H(\mathbf{r}) < 0$, see the Supporting Information **S3**. This result is consistent with the low, but non-zero, value of $K \approx 0.2$ and high value of $K' \approx 0.8$, see Figure 3A and Figure 3B respectively. For the undoped DTE fatigue C5—C11 bond-path the large and minor peaks in the ellipticity ε profile at $\approx \pm 1.2$ au along the bond-path coincide with the minima in the Laplacian $\nabla^2\rho(\mathbf{r})$ profile, see Figures 2A and 3A,B respectively. Similarly, for the sulfur doped DTE, the peaks in the fatigue C5—S26 *BCP* bond-path ellipticity ε profile at $\approx \pm 0.9$ au also correspond to the minima in the Laplacian $\nabla^2\rho(\mathbf{r})$ profile, see Figures 2B and 3C,D respectively.

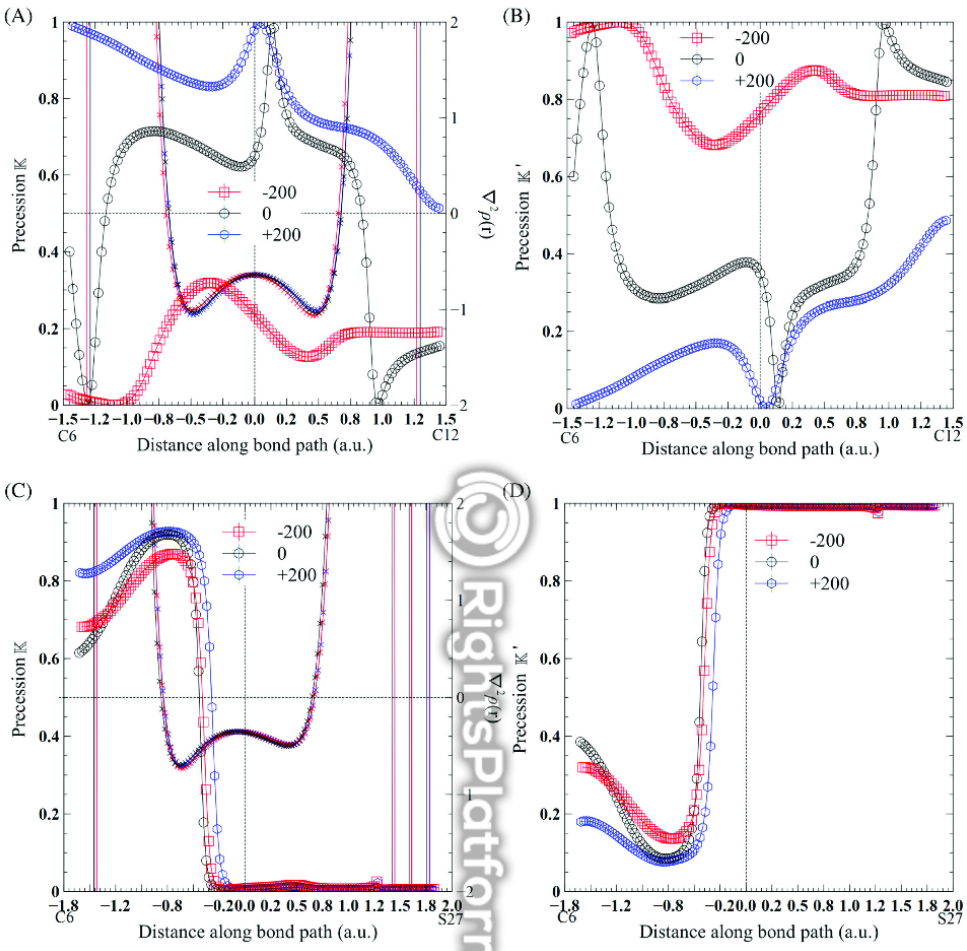

FIGURE 5 The values of the C6—C12 bond critical point (*BCP*) bond-path {***p***,***p***′} and {***q***,***q***′} path-packet precession *K* and *K*′ for the undoped DTE are presented in sub-figure (A) and (B) respectively. The values of the C6—S27 *BCP* bond-path {***p***,***p***′} and {***q***,***q***′} precession *K* and *K*′ for the sulfur doped DTE are presented in sub-figure (C) and (D) respectively, see the caption of Figure 3 for further details

The fatigue shared-shell C5—S26 *BCP* bond-path precessions *K* and *K*′ of the {***p***,***p***′} and {***q***,***q***′} path-packets demonstrates "pure" and unmixed chemical character at the location of the fatigue C5—S26 *BCP*, that is, only shared-shell character on the basis of *K* = 0 and *K*′ = 1, see Figure 3A,B respectively.

The DTE shared-shell C7—C11/C7—S26 *BCP* bond-paths are orientated approximately perpendicularly to the corresponding fatigue C5—C11/C5—S26 *BCP* bond-paths, see Figure 1. It can see seen that the precessions *K* and *K*′ are significantly affected by the applied $\boldsymbol{E}_{\text{para}}$-field with the *K* values associated with the C7—C11 *BCP* bond-path. In particular, we see a significant relative increase in closed-shell character for the $\boldsymbol{E}_{\text{para}}$-field = −0.02 au and decrease for $\boldsymbol{E}_{\text{para}}$-field = +0.02 au, see Figure 4A. The corresponding shared-shell C7—C11 *BCP* bond-path displays a significant relative *decrease* in shared-shell character for the $\boldsymbol{E}_{\text{para}}$-field = −0.02 au and increase for $\boldsymbol{E}_{\text{para}}$-field = +0.02 au, see Figure 4B. The very low closed-shell character in the absence of the $\boldsymbol{E}_{\text{para}}$-field seen from the precessions *K* close to the C7 *NCP* for the C7—S26 *BCP* bond-path, is not apparent in the presence of the $\boldsymbol{E}_{\text{para}}$-field, see Figure 4C. The converse being true for the *K*′ for the C7—S26 *BCP* bond-path, see Figure 4D.

The C6—C12 *BCP* bond-path is the most affected of the selected bond-paths, along the entire extent of the bond-path, by the application of the $\boldsymbol{E}_{\text{para}}$-field = ± 0.02au, see Figure 5A,B. In particular, the shared-shell C6—C12 *BCP* that comprises significant closed-shell character for $\boldsymbol{E}_{\text{para}}$-field = +0.02au and the absence of the $\boldsymbol{E}_{\text{para}}$-field but much lower closed-shell character the $\boldsymbol{E}_{\text{para}}$-field = −0.02au, see Figure 5A. This is presented

RightsPlatform